Radiol Phys Technol (2012) 5:78–85
DOI 10.1007/s12194-011-0139-9

Image-quality assessment method for digital phase-contrast imaging based on two-dimensional power spectral analysis

Satoru Matsuo · Junji Morishita · Tetsuro Katafuchi · Chika Honda · Hiroshi Fujita

Received: 19 April 2011 / Revised: 21 October 2011 / Accepted: 24 October 2011 / Published online: 10 November 2011

Abstract With use of the phase shift of X-rays that occurs when they pass through an object, phase-contrast imaging (herein referred to as "phase imaging") can produce images different from those of conventional contact imaging (herein referred to as "conventional imaging"). For this reason, assessment of the image quality based on noise-equivalent quanta (NEQ) and detective quantum efficiency (DQE) which does not include object-based information may not be appropriate for comparison of image quality between phase and conventional images. As an alternative method, we conceived a new image-quality assessment method with images that contain information about an object. First, we constructed images with an object and without an object under the same imaging parameters; then, we obtained two-dimensional power spectra by Fourier transform of those images. Second, we calculated the radial direction distribution function with the power spectra, and the distribution of signal intensity, which we defined as a signal intensity distribution function (SIDF). In this way, differences in image quality were evaluated relatively based on the SIDF of the imaged object. In our study, we first confirmed that phase-imaging evaluation was not appropriate by comparing NEQ and DQE of conventional, magnification, and phase imaging. Further, comparing the image quality of projected plant seeds by employing conventional, magnification, and phase imaging, we found that the phase-imaging method provided a higher image quality regarding edge sharpness than did conventional and magnification imaging. Therefore, based on these results, our image assessment method is considered useful for evaluation of images which include object-based information.

Keywords Phase-contrast imaging · Two-dimensional power spectrum · Signal intensity distribution function · Radial direction distribution function · Image quality

S. Matsuo (✉)
Department of Radiology, Shiga University of Medical Science, Seta Tsukinowa-cho, Otsu, Shiga 520-2192, Japan
e-mail: matsuo@belle.shiga-med.ac.jp

J. Morishita
Department of Health Sciences, Faculty of Medical Sciences, Kyushu University, 3-1-1 Maidashi, Higashi-ku, Fukuoka, Fukuoka 812-8582, Japan

T. Katafuchi
Department of Radiological Technology, Gifu University of Medical Science, 795-1 Nagamine Ichihiraga, Seki, Gifu 501-3892, Japan

C. Honda
The Society of Photographic Science and Technology of Japan, 2-9-5 Hon-machi, Nakano-ku, Tokyo 164-8678, Japan

H. Fujita
Department of Intelligent Image Information, Graduate School of Medicine, Gifu University, 1-1 Yanagido, Gifu, Gifu 501-1194, Japan

1 Introduction

When X-rays pass through an object, the X-ray energy is absorbed in the object due to the photoelectric effect and Compton scattering. The image density difference relative to the X-ray energy absorption is called the "absorption contrast", which is the principle of radiograph formation. Further, phase shift occurs after X-rays pass through an object, and the image density difference arising from the phase shift is called "phase contrast". The X-ray imaging which delineates the phase contrast is called "X-ray phase-contrast imaging" (herein referred to as "phase imaging")

[1, 2]. Phase imaging is intended to provide edge enhancement (phase effect) of an imaged object, utilizing refracted X-rays which occur when X-rays pass through the object [3–10].

Evaluation of phase imaging by use of a small-focal-spot X-ray tube has been reported by several researchers. Kotre et al. [11] reported visual evaluation of mammographic images of a TORMAM image-quality phantom using three imaging methods, i.e., conventional contact imaging (conventional imaging), magnified imaging (magnification imaging), and digital phase-contrast imaging (phase imaging). Gido et al. [12] measured the modulation transfer function (MTF), Wiener spectrum (WS) (noise power spectrum), and noise-equivalent quanta (NEQ) of a phase-contrast mammography (PCM) system. Yamazaki et al. [13] studied the MTF and digital WS of a PCM system, calculated the response function from image profile curves, and compared with those of conventional imaging. However, the phase effect derived from refracted X-rays was not discussed sufficiently in these reports because they used simple objects (metallic plates or simple acrylic objects) for measurement, which were different from actual images [12, 13]. Kuhis-Gilcrist et al. [14] introduced a new technique to determine the system pre-sampled MTF in digital radiography using only the WS, although calculation of the MTF, including the phase effect, is not possible.

For image evaluation in digital X-ray imaging systems, NEQ and detective quantum efficiency (DQE) [15, 16] arising from the concept of the signal-to-noise ratio (SNR) cannot be applied to images with an edge-enhancement effect produced by refracted X-rays, as these measures are calculated by the MTF and WS without consideration of the phase effect. Therefore, for image quality evaluation of phase imaging, we need to investigate the X-ray intensity distribution after it passes through an imaged object, including refracted X-ray effects.

As one of the evaluation methods that include an imaged object, we conceived a new image evaluation method in the present study, utilizing the signal intensity distribution function (SIDF) which was obtained based on a two-dimensional (2D) power spectrum (herein referred to as "power spectrum") [17–21]. Our method utilizing the power spectrum of an imaged object is a comprehensive method for single evaluation of the capability of an imaging system by a combination of contrast, sharpness, and noise characteristics.

This evaluation method enables the comparison of images including an imaged object by direct spectral analysis, in which the spectrum difference indicates the imaged object's data information. However, components of power spectrum frequencies obtained from an X-ray beam passing through the object include X-ray quantum noise and system noise; thus, we cannot solely study the important signals of phase images. Therefore, we surmised that the analysis of spatial-frequency components of image signals would be possible by a comparison of the power spectrum of the noise component without including an object (namely, the "noise power spectrum") with that of the signal and the noise components.

Firstly, we evaluated the image quality of conventional, magnification, and phase imaging (without including phase effect) by NEQ and DQE, in which we confirmed that the image quality of phase imaging was not evaluated appropriately. Secondly, we produced and evaluated X-ray images of plant seeds by conventional, magnification, and phase imaging, in order to analyze the image improvement due to the re-scaling effect (magnification effect) and phase effect (edge enhancement).

2 Experimental methods

2.1 X-ray imaging

The system used in our experiment (Mermaid, Konica Minolta, Tokyo, Japan) consisted of mammography X-ray equipment (MGU-100B, Toshiba, Tokyo, Japan) capable of performing conventional imaging (Fig. 1a), magnification imaging (Fig. 1b), and phase imaging (Fig. 1c), and a data reader (REGIUS MODEL190, Konica Minolta, Tokyo, Japan). A photostimulable phosphor plate (RP-6M, Konica Minolta, Tokyo, Japan) was used as the X-ray detector.

All images were obtained with use of a molybdenum X-ray tube having a focal spot 0.1 mm in diameter. In conventional and phase imaging, the distance between the focal spot of the X-ray tube and the target object was 65 cm. In conventional imaging, the detector was positioned directly behind the object, whereas in phase imaging, the detector was positioned 49 cm away from the object. In magnification imaging, the distance between the focal spot of the X-ray tube and the imaged object was 37 cm, and the distance between the imaged object and the detector was 28 cm. Therefore, in magnification and phase imaging, the imaged object was magnified 1.75 times.

The digital imaging system had a sampling pitch of 0.04375 mm and a density resolution of 12 bits. Therefore, the effective sampling pitch at 1.75 times magnification with phase imaging was 0.025 mm.

2.2 Evaluation by NEQ and DQE

The characteristics of image quality were compared by NEQ and DQE for conventional, magnification, and phase imaging. NEQ (u, v) was calculated by Eq. 1 that included the MTF_P (u, v), which was the pre-sampled MTF excluding the effects of aliasing of the digital system, and WS_D (u, v), which was a digital Wiener spectrum [15, 16].

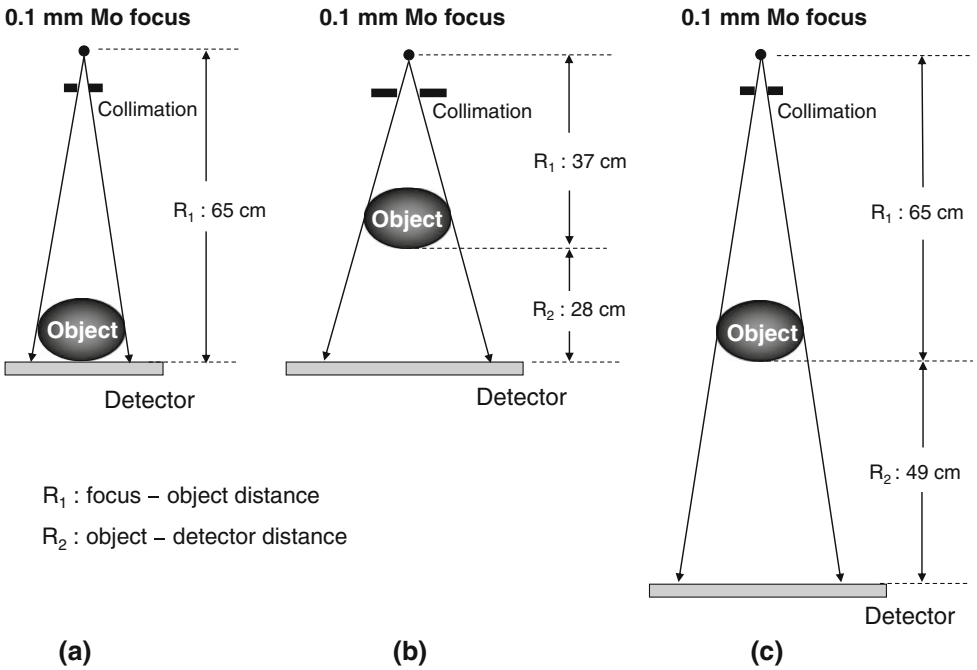

Fig. 1 Geometric conditions employed in this study. **a** Conventional imaging, **b** 1.75 times magnification imaging, and **c** 1.75 times phase imaging

$$\mathrm{NEQ}(u,v) = (S/N)_{\mathrm{OUT}}{}^2(u,v) = \frac{\mathrm{MTF}_{\mathrm{P}}^2(u,v)}{\mathrm{WS}_{\mathrm{D}}(u,v)}. \quad (1)$$

DQE (u, v) was calculated by Eq. 2 from the number of incident photons "q" per unit area [15, 16].

$$\mathrm{DQE}(u,v) = \frac{(S/N)_{\mathrm{OUT}}{}^2}{(S/N)_{\mathrm{IN}}{}^2} = \frac{\mathrm{MTF}_{\mathrm{P}}^2(u,v)}{q \times \mathrm{WS}_{\mathrm{D}}(u,v)}. \quad (2)$$

$\mathrm{MTF_P}$ (u, v), which was used for calculation of NEQ (u, v) and DQE (u, v), is an image resolution characteristic specific for the digital system [22–24] excluding object-based information.

Measurements of the digital characteristic curves necessary for calculation of NEQ and DQE, the MTF (pre-sampled MTF by the edge method), and the WS (2D Fourier transform method) were done according to IEC (International Electrotechnical Commission) 62220-1 Ed.1 [25], which is a standard for DQE measurement of digital X-ray imaging input systems for clinical use. Standard radiation quality [Mo/Mo (RQA-M2): 28 kV] was applied to all images, according to the definition of the IEC 61267 (Medical diagnostic X-ray equipment-radiation condition for use in the determination of characteristics). The MTF of magnification and phase imaging was calculated from the MTF of conventional imaging, considering the re-scaling effect and the effect of geometrical unsharpness due to the diameter of the X-ray focal spot. The geometric unsharpness associated with the diameter of the focal spot was calculated assuming that the intensity distribution in the X-ray focal spot had a Gaussian distribution (FWHM = 0.1 mm: focal spot size) [26]. To obtain the WS, we used imaging parameters of 28 kV (tube voltage) and 40 mAs (exposure dose) for both conventional and magnification imaging samples, and 28 kV (tube voltage) and 120 mAs (exposure dose) for phase imaging samples. Three samples were produced for each imaging method. Under these conditions, the exposure dose to the X-ray detector was the same, approximately 230 μGy for each of the three imaging methods. Then, the WS of the magnification imaging was calculated according to the Eq. 3 [27]:

$$\mathrm{WS_m}(u,v) = \frac{1}{m^2}\mathrm{WS_c}\left(\frac{u}{m},\frac{v}{m}\right), \quad (3)$$

where $\mathrm{WS_m}$ (u, v) is the WS of magnification imaging, $\mathrm{WS_c}$ (u, v) is the WS of conventional imaging, and m is the magnification ratio.

2.3 Power spectrum evaluation

2.3.1 Evaluation methods

Supposing a digital image of g (m, n), in which the picture elements (pixels) are aligned in the x axis direction by the number M, and in the y axis by the number N, the 2D Fourier transform of G (u, v) is expressed by Eq. 4 [19]:

$$G(u,v) = \frac{1}{\sqrt{MN}}\sum_{m=0}^{M-1}\sum_{n=0}^{N-1} g(m,n)\exp\left\{-j2\pi\left(\frac{mk}{M}+\frac{nl}{N}\right)\right\}, \quad (4)$$

where j is a complex number ($=\sqrt{-1}$). The power spectrum of G (u, v), i.e. P (u, v), is expressed by Eq. 5, the value of which shows a squared number (energy) of the amplitude at the spatial frequency (u, v) [19]:

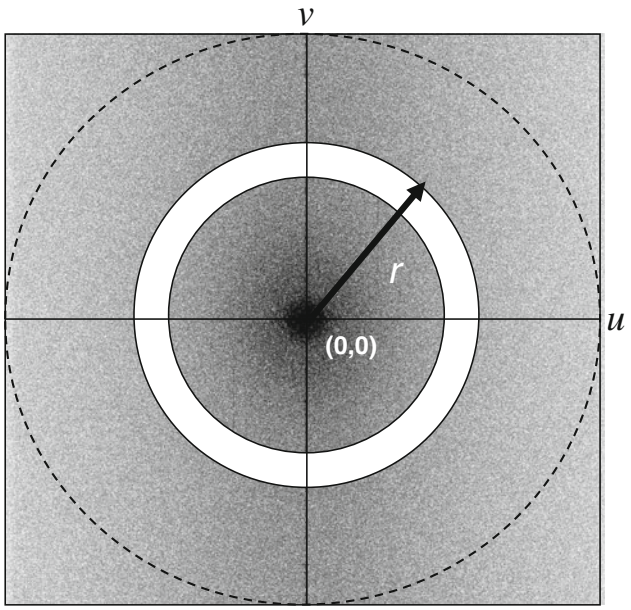

Fig. 2 The concept of the radial direction distribution function (RDDF) of the spectrum, p (r): the ingredient of frequency r is extracted

$$P(u,v) = |G(u,v)|^2, \tag{5}$$

where P (u, v) can be expressed as P (r, θ) by the polar coordinates centered at the origin at (u, v) = (0, 0), with the distance (r) and direction (θ). As shown in Eq. 6, the sum total of components at the spatial frequency (r), which is p (r) (showing the roughness of the texture and the size of the object being imaged), is considered [19, 20]:

$$p(r) = 2\sum_{\theta=0}^{\pi} P(r,\theta), \tag{6}$$

where p (r) is the sum total of the power spectrum in the spatial-frequency regions; a round shape as shown in Fig. 2. A large p (r) indicates a large power spectrum component in the spatial frequency corresponding to r, and there is a regular repetition of darkness and lightness, corresponding to the spatial frequency of an image. Namely, p (r) is defined as the radial direction distribution function (RDDF) that shows the degree of textural roughness.

Next, as shown in Eq. 7, by use of a logarithm of the ratio between the p_{s+n} (r) of the "signal + noise component" image and p_n (r) of the "noise component" image, the subtraction of p_n (r) from p_{s+n} (r) is performed, and, thus, the RDDF of only "signals" is obtained (supposing approximation is possible by only an additive noise component). In the present study, we defined it as the SIDF, i.e. P_s (r) [18]:

$$P_s(r) = 10\log_{10}\frac{p_{s+n}(r)}{p_n(r)}\ [\mathrm{d}B]. \tag{7}$$

Here, note that both images have to be obtained by use of the same exposure conditions.

2.3.2 *Production of sample images for measurement*

The image quality of conventional, magnification, and phase images was compared with use of plant seeds (including grains of rice embedded in glue) having major axes of 4–5 mm (Fig. 3). In order to keep the entrance dose to the detector the same in the comparison, we set the exposure conditions of the phantom for conventional imaging (Fig. 1a) and magnification imaging (Fig. 1b) at a tube voltage of 28 kV and 5 mAs; that for phase imaging (Fig. 1c) was set at the same voltage of 28 kV, but with 16 mAs. In the present study, "noise images" were defined as images obtained with the same exposure conditions but without use of a phantom, for measurement of the noise component only. Three samples were made for each method. For clinical mammography with conventional imaging, a grid is generally used for reduction of scattered X-rays. However, such a grid was not used in the present study for conventional, magnification, and phase imaging, because the scattered X-rays from the phantom were negligible. We evaluated quality differences of conventional, magnification, and phase imaging using the RDDF and SIDF of plant seed images.

3 Results

3.1 NEQ and DQE

The MTF and WS of conventional, magnification, and phase imaging are shown in Fig. 4a and b, respectively. In the low-frequency band, the MTF of magnification imaging was greater than that of conventional imaging due to the re-scaling effect, whereas in the high-frequency band, the MTF of magnification imaging was less than that of conventional imaging due to geometric unsharpness. As for the WS, the noise property improved in magnification imaging over conventional imaging, because of the magnification. As shown in Eq. 3, the noise property has been known to be improved in magnification imaging, compared with conventional imaging (the dose incident on the detector is the same for the two imaging methods) [26]. The WS of magnification imaging calculated by Eq. 3, based on the WS of conventional imaging, showed agreement between the actually measured WS of magnification and that of phase imaging.

The NEQ and DQE calculated from the MTF and WS are shown in Fig. 5a and b, respectively. Higher NEQ and DQE

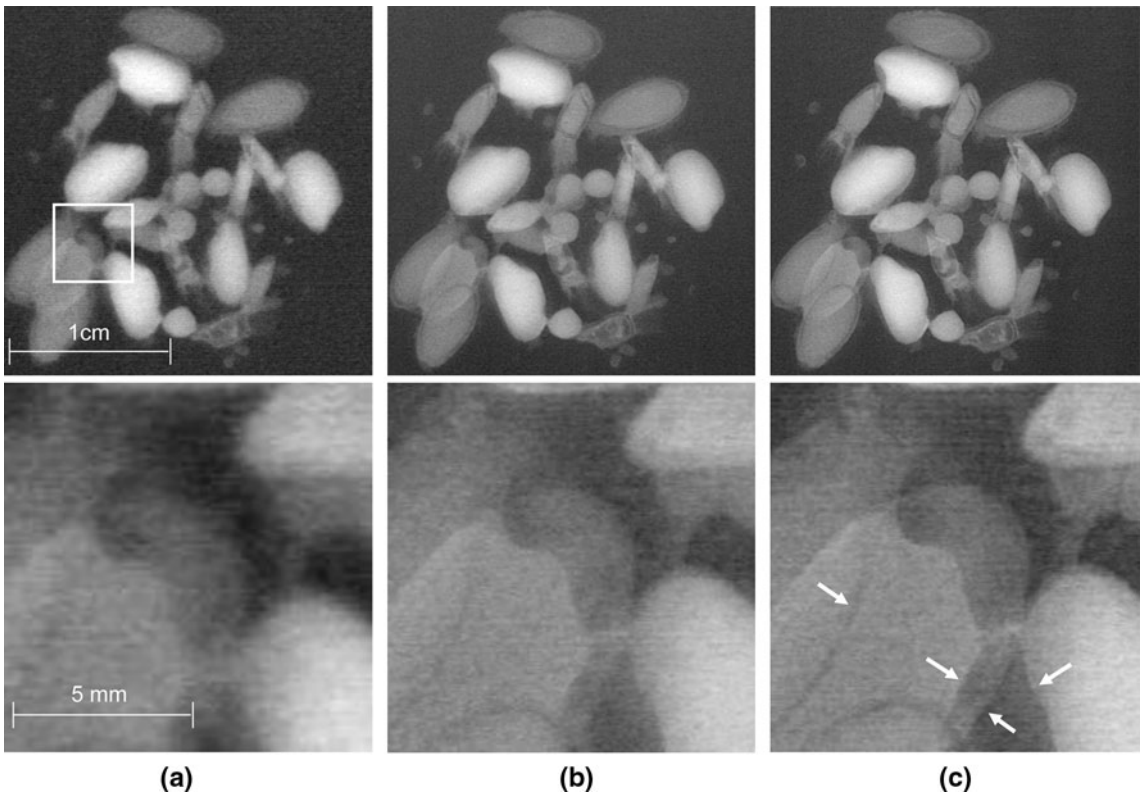

Fig. 3 Images of plant seeds embedded in glue (having major axes of 4–5 mm). **a** Conventional image, **b** 1.75 times magnification image, and **c** 1.75 times phase image. Lower images are magnified images on the *white-box* region in each of the upper images. (Note that 0.04375 mm ÷ 0.025 mm = 1.75, which is the magnification ratio in the magnification and phase imaging.)

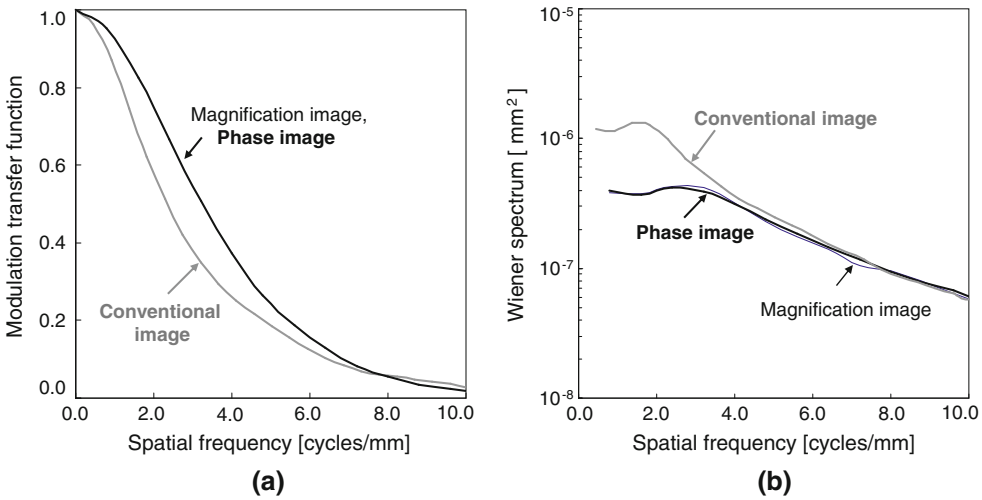

Fig. 4 MTFs in (**a**), WSs in (**b**) of the conventional imaging, 1.75 times magnification imaging, and 1.75 times phase imaging

were found in magnification and phase imaging, compared with those in conventional imaging. The NEQ and DQE of magnification and phase imaging were the same.

3.2 Power spectrum evaluation

The RDDF and SIDF of the conventional, magnification, and phase images as shown in Fig. 3 are exhibited in Figs. 6a and b, respectively.

Based on the RDDF shown in Fig. 6a, the power spectrum of plant seeds imaged at each frequency was found to be larger in conventional images than that of magnification or phase images. In background-noise images, the RDDF of magnification images was high in the low-spatial-frequency band of 0.7 cycle/mm, and the RDDF of conventional images was high when the spatial-frequency band exceeded 0.7 cycle/mm. The RDDF of phase images was low in every spatial-frequency band. The reason for the high RDDF of magnification images

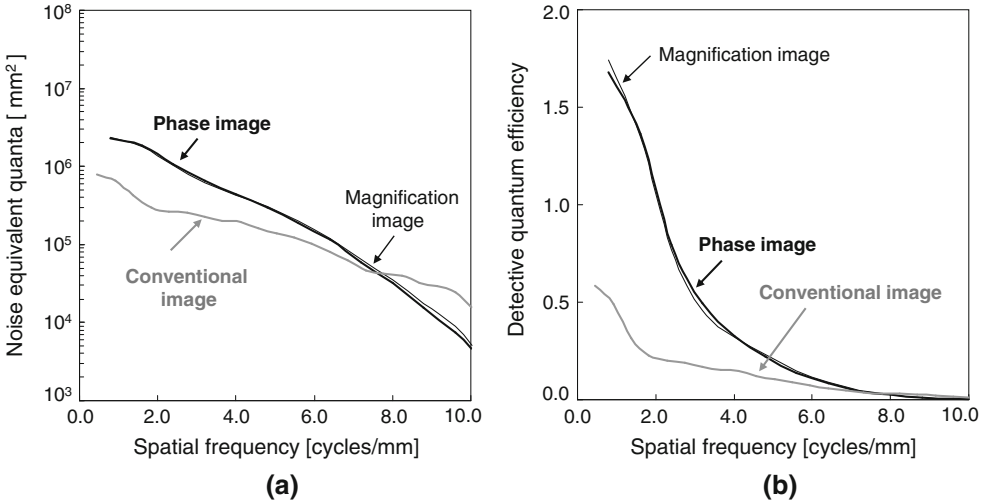

Fig. 5 NEQs in (**a**), and DQEs in (**b**) of the conventional imaging, 1.75 times magnification imaging, and 1.75 times phase imaging

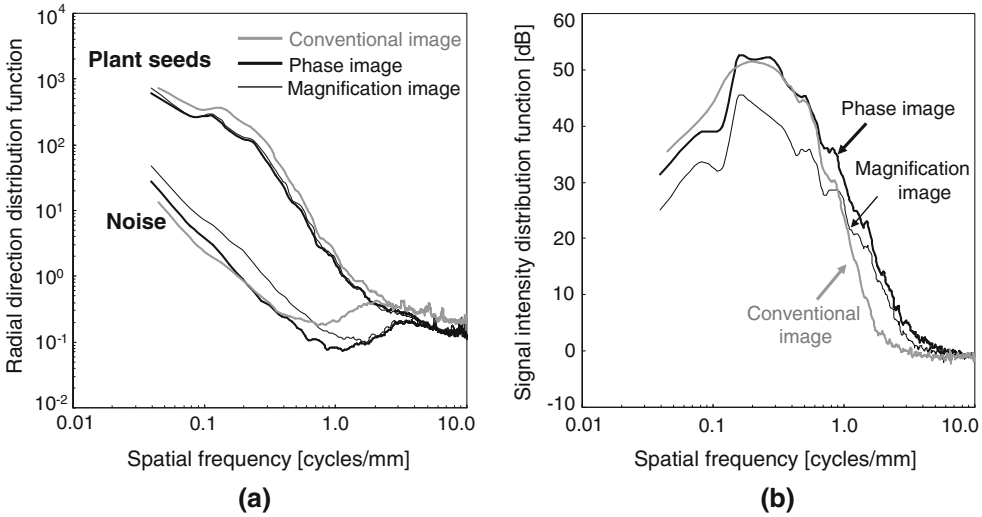

Fig. 6 Radial direction distribution functions (RDDFs) of plant seeds and noise images for conventional, magnification, and phase imaging (**a**). Signal intensity distribution functions (SIDFs) of plant seed images for conventional, magnification, and phase imaging (**b**)

in the low-frequency band of less than 0.7 cycle/mm is the influence of the heel effect, which is specific for the X-ray tube of a mammography system. For the geometric arrangement of magnification imaging (shown in Fig. 1), a 1.75 times wider X-ray band is necessary to yield the same exposure field as that for conventional or phase imaging. Therefore, magnification imaging tends to be influenced by the heel effect, compared with conventional or phase imaging.

Based on the SIDF shown in Fig. 6b, the signal intensity of magnification imaging was inferior to that of conventional or phase imaging in the low-spatial-frequency band (0.7 cycle/mm or less). In spatial-frequency bands exceeding 0.7 cycle/mm, the signal intensity of phase imaging was better than that of conventional imaging.

4 Discussion

The improvement of sharpness found in phase imaging can be explained by the re-scaling effect due to magnification imaging and the phase effect due to refracted X-rays.

For an X-ray tube with a small focal spot (0.1 mm), the desired geometric arrangement of an object has been known to obtain edge-enhancement images with refracted X-rays [7]; the conditions necessary for verification of the edge-enhancement effect are source-to-object distance (R_1) $\geq$ 50 cm and an object-to-detector distance (R_2) $\geq$ 25 cm, as shown in Fig. 1. Even at the same magnification ratio, the edge-enhancement effect occurs in geometrical arrangement as shown in Fig. 1c, although such edge-enhancement effect does not occur in the geometric arrangement shown in Fig. 1b. Therefore, the differences in image quality between Fig. 3a and b are considered to be due to the presence or absence of the re-scaling effect, whereas the differences in image quality between Fig. 3b and c are considered to be due to the presence or absence of the phase effect.

Evaluation based on NEQ or DQE can assess the re-scaling effect, but it cannot assess the phase effect. Therefore, MTF measurement including the phase effect is

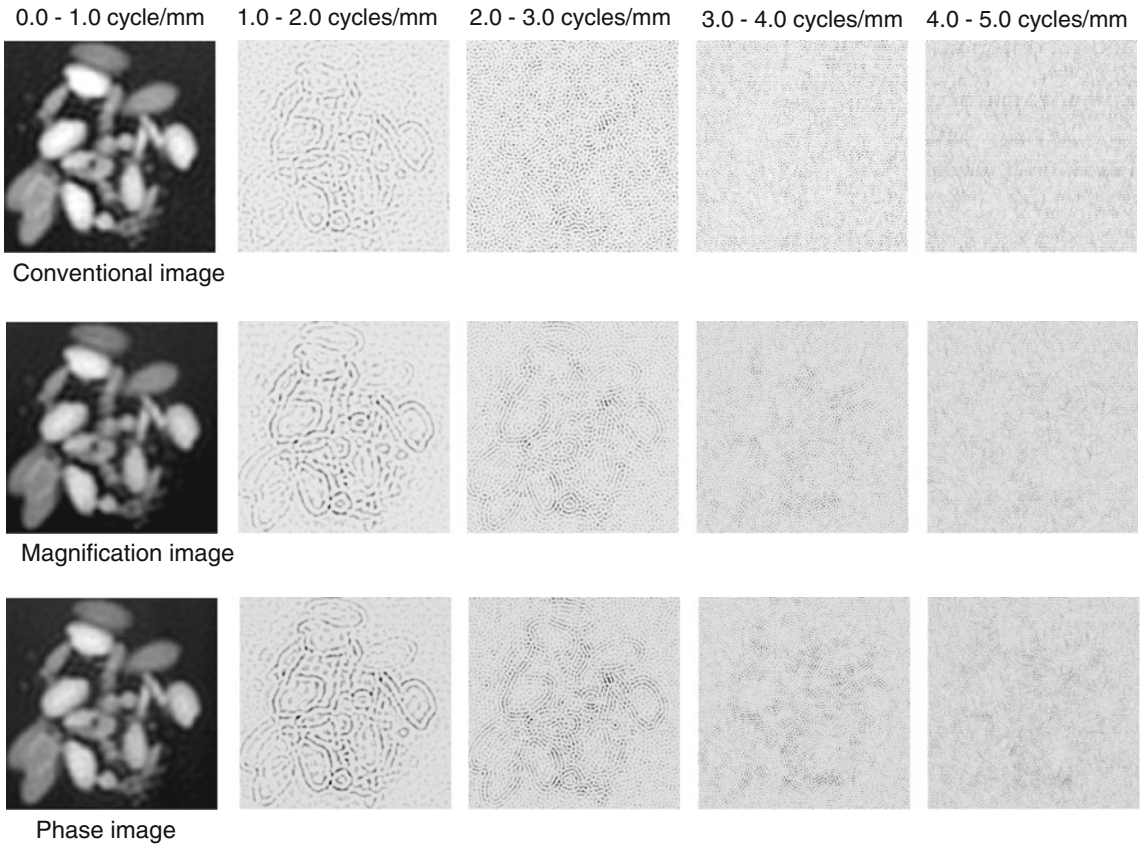

Fig. 7 Decomposed images of plant seeds (Fig. 3) obtained on conventional, magnification, and phase images processed with the band-pass filter. Although the image component of the phase and magnification images can be confirmed visually over the frequencies at least up to 5.0 cycles/mm, that of conventional images cannot be seen at a frequency band higher than 3.0 cycles/mm

necessary. However, it is difficult to reflect the phase effect in the MTF, because the phase effect changes depending on the material, shape, size, and location of the object being imaged.

The power spectrum method used in our study is a comprehensive image evaluation method based on the comparison of the spatial-frequency spectrum of images including an object. However, with the present method, the possible area for evaluation is limited to a specific spatial-frequency band which includes signals of an imaged object. Unlike an absolute evaluation method without use of an imaged object, such as the NEQ and DQE, the power spectrum evaluation is a relative evaluation method subject to the SIDF changes relative to the imaged object.

We performed filtering processing to evaluate differences in the SIDF spectrum on actual spatial images, as shown in Fig. 6b. Band-pass filter processing (band width: 1.0 cycle/mm) was performed for spatial-frequency images obtained by Fourier transform of plant seed images by conventional, magnification, and phase imaging; we then returned to actual space images by use of the inverse 2D-Fourier transform, as shown in Fig. 7. Band-pass filter processing was conducted with a band width of 1.0 cycle/mm and a frequency band of 0.0–5.0 cycles/mm. Thus, five kinds of images were obtained after frequency analysis. The image contrast had already been determined in the low-frequency bands of 0.0–1.0 cycles/mm in conventional, magnification, and phase imaging. Although the image component of phase and magnification images can be confirmed visually over the entire frequencies at least up to 5.0 cycles/mm, that of conventional images cannot be seen at a frequency band higher than 3.0 cycles/mm.

Phase imaging with a digital X-ray detector in our study could not produce edge-enhanced images as was seen in phase imaging with use of an analogue X-ray detector [4, 5]. The cause was that the edge-enhancement effect was reduced, because the resolution characteristic of a photostimulable phosphor plate of computed radiography was much inferior to that with an intensifying screen-film system. Recently, a flat-panel detector became available, which is based on a direct-conversion technique with high precision and an excellent resolution property, thus further improvement of image quality is hoped for by phase imaging with use of such a digital X-ray detector.

5 Conclusion

In the present study, we investigated whether image-quality evaluation was possible among different images, by use of the RDDF and SIDF, which were obtained from the power spectrum.

Our method was proved to be able to evaluate the sharpness of images considering the noise component, through our image-quality evaluation results of conventional, magnification, and phase images. Also, we found that phase imaging enabled a substantial improvement of the images.

However, the power spectrum method is a kind of relative evaluation depending on the object-based information, unlike an absolute evaluation method, such as the use of NEQ and DQE. For absolute evaluation by NEQ or DQE, further investigation by the utilization of an MTF measurement method including the phase effect is needed in future studies.

Acknowledgments The authors appreciate fruitful discussions with Mr. Hiromu Ohara of Konica Minolta Medical and Graphic, Inc. We also thank Prof. Kiyoshi Murata of the Shiga University of Medical Science and Mr. Masatake Imai of the Shiga University of Medical Science Hospital for their permission to publish this work.

References

1. Wilkins SW, Gureyev TE, Gao D, Pogany A, Stevenson AW. Phase-contrast imaging using polychromatic hard X-rays. Nature. 1996;384:335–8.
2. Fitzgerald R. Phase-sensitive X-ray imaging. Phys Today. 2000;53:23–6.
3. Tohyama K, Katafuchi T, Matsuo S, Morishita J, Yamada K. Application of phase contrast imaging to mammography. Jpn J Radiol Technol. 2005;61:245–52.
4. Tohyama K, Katafuchi T, Matsuo S. Clinical implications of phase-contrast imaging in mammography. Jpn J Med Imaging Inf Sci. 2006;23:79–84.
5. Matsuo S, Katafuchi T, Tohyama K, Morishita J, Yamada K, Fujita H. Evaluation of edge effect due to phase contrast imaging for mammography. Med Phys. 2005;32:2690–7.
6. Matsuo M, Morishita J, Fujita H, Katafuchi T, Sugiyama J. Evaluation of edge enhancement in a digital phase contrast imaging. Jpn J Med Imaging Inf Sci. 2006;23:120–3.
7. Ishisaka A, Ohara H, Honda C. A new method of analyzing edge effect in phase contrast imaging with incoherent X-rays. Opt Rev. 2000;7:566–72.
8. Honda C, Ohara H, Ishisaka A, Shimada F, Endo T. X-ray phase imaging using a X-ray tube with a small focal spot-improvement of image quality in mammography. Jpn J Med Phys. 2002; 22:21–8.
9. Donnelly EF, Price RR. Quantification of the effect of kVp on edge-enhancement index in phase-contrast radiography. Med Phys. 2002;29:999–1002.
10. Matsuo S, Fujita H, Morishita J, Katafuchi T, Honda C, Sugiyama J. Evaluation of a phase contrast imaging with digital mammography. In: Krupinski EA, editors. Digital mammography. Springer Lectures Notes in Computer Science (LNCS) series, vol 5116. Berlin: Springer; 2008. p. 130–6.
11. Kotre CJ, Birch IP, Robson KJ. Anomalous image quality phantom scores in magnification mammography: evidence of phase contrast enhancement. Br J Radiol. 2002;75:170–3.
12. Gido T, Nagatsuka S, Amitani K, Yonekawa H, Shimoji M, Honda C. Advanced digital mammography system based on phase contrast technology. Proc SPIE. 2005;5745:511–8.
13. Yamazaki A, Ichikawa K, Kodera Y. Investigation of physical image characteristics and phenomenon of edge enhancement by phase contrast using equipment typical for mammography. Med Phys. 2008;35:5134–50.
14. Kuhis-Gilcrist A, Jain A, Bednarek D, Rudin S. Accurate MTF measurement in digital radiography using noise response. Med Phys. 2010;37:324–735.
15. Shaw R. Evaluating the efficiency of imaging processes. Rep Prog Phys. 1978;41:1103–55.
16. Beutel J, Kundel HL, Van Metter RL. Handbook of medical imaging, vol 1. Physics and psychophysics. Washington: SPIE Press; 2000.
17. Onishi H, Takahashi M, Matsuo S, Ushio N, Noma N, Masuda K. Evaluation of a SPECT image using a textual analysis. Jpn J Radiol Technol. 1995;51:710–6.
18. Matsuo S, Komizu M, Kida T, Noma K, Hashimoto K, Onishi H, Masuda K. Analysis of frequency components of X-ray images. Jpn J Radiol Technol. 1997;53:1665–72.
19. Pratt WK. Digital image processing. Canada: Wiley; 1978. p. 473–7.
20. Gonzalez RC, Wintz P. Digital image processing. Canada: Addison-Wesley; 1987. p. 418.
21. Rangayyan RM. Biomedical image analysis. Florida: CRC Press; 2000. p. 612–21.
22. Giger ML, Doi K. Investigation of basic imaging properties of digital radiography. 1. Modulation transfer function. Med Phys. 1984;11:287–95.
23. Fujita H, Doi K, Giger ML. Investigation of basic imaging properties in digital radiography. 6. MTFs of I.I-TV digital imaging systems. Med Phys. 1985;12:712–20.
24. Fujita H, Tsai DY, Itho T, Doi K, Morishita J, Ueda K, Ohtsuka A. A simple method for determining the modulation transfer function in digital radiography. IEEE Trans Med Imaging. 1992;11:34–9.
25. IEC 62220-1-2. Medical electrical equipment – characteristics of digital X-ray imaging devices – part 1–2: determination of the detective quantum efficiency – detectors used in mammography; 2007. p. 3–27.
26. Matsuo S, Onishi H, Noma K, Kida T, Komizu M, Masuda K. Evaluation of resolution of scintillation camera using presampling MTF. Jpn J Radiol Technol. 1997;53:460–6.
27. Doi K, Imhof H. Noise reduction by radiographic magnification. Radiology. 1977;122:479–87.